Supporting Information

Daranlot et al. 10.1073/pnas.1200017109

SI Text

Experimental cross-checks. Early test experiments at 152 K showed that the pseudo-first-order decay curves of the OH radicals such those shown in Fig. 2 did not vary as a function of the ICN concentration. In contrast, it was seen that under certain conditions, the CN radical fluorescence signal did not decay to zero at long times, but instead to a non-zero baseline value. This residual signal varied as a function of the gas-phase H_2O_2 (or H_2O) concentration, so that at high concentrations of H_2O_2, the CN fluorescence signal decayed to the pre-trigger zero level. At low H_2O_2 concentrations, the baseline value was as large as 9% of the peak signal amplitude. When the values of k'_4 determined from fits to decays measured in the presence of low $[H_2O_2]$ were plotted as a function of the corresponding k'_1 value, the ratio k_4/k_1 was seen to be larger than the ratio determined at high $[H_2O_2]$. Several test experiments under conditions identical to those used in these early experiments were performed to determine the origin of this effect. Using a solar blind channel photomultiplier tube (Perkin Elmer MP1911) in photon counting mode coupled to a monochromator with a grating blazed at 121 nm, it was possible to observe emission from excited $A^3\Sigma_u^+$ molecular nitrogen N_2^* within the supersonic flow at several wavelengths between 145 and 185 nm. The emission intensity was seen to vary strongly as a function of $[H_2O_2]$ within the flow, with little or no emission occurring at the highest $[H_2O_2]$.

In light of these findings, further test experiments employing CBr_4 as a precursor for $C(^3P)$ atoms were performed at 152 K. Here, CBr_4 was entrained in the supersonic flow and underwent pulsed multi-photon dissociation at 266 nm. No other minor reagent precursor molecules were used, atomic nitrogen was produced in the usual manner (thereby producing N_2^*), and the probe laser was tuned to a CN $B^2\Sigma^+$-$X^2\Sigma^+$ transition. Under these conditions, formation of CN radicals was clearly observed in the supersonic flow. Moreover, the rate of production of CN varied as a function of the atomic nitrogen concentration (tested by varying the N_2 flow through the discharge and/or the discharge power). This last observation indicates that the rate of formation of CN is strongly linked to $[N_2^*]$. We postulate that the following process may have led to secondary CN formation:

$$C(^3P) + N_2^* \rightarrow CN + N, \qquad \textbf{[S1]}$$

with atomic carbon being formed as the primary product of reaction 4. Given the experimental evidence, two possible mechanisms are potentially responsible for inhibiting reaction **S1**, leading to zero residual baseline values. Firstly, it is probable that N_2^* is either quenched or reacts with H_2O_2 or H_2O given the dependence of the emission intensity on $[H_2O_2]$ or $[H_2O]$. Secondly, we cannot rule out the possibility that $C(^3P)$ is also removed by reaction with H_2O_2. In both cases, high $[H_2O_2]$ would lead to less secondary CN formation. As a result, all experiments used in the final analysis were those conducted with $[H_2O_2]$ greater than 3.9×10^{12} cm^{-3}.

Although reaction 4 from ground state reactants $N(^4S^0)$ and $CN(^2\Sigma^+)$ leading to ground state products $C(^3P)$ and $N_2(^1\Sigma_g^+)$ is exothermic by 191.4 kJ mol^{-1}, the formation of excited state $C(^1D)$ is also energetically possible (although the products no longer correlate adiabatically with the reactants), with an exothermicity of 69.3 kJ mol^{-1}. As a result, further test experiments were performed at 152 K to check for the presence of these atoms. Unlike $C(^3P)$, $C(^1D)$ is known to react rapidly with H_2 at room temperature to form methylidyne radicals (1), CH, which should themselves react with $N(^4S^0)$ to reform CN radicals (reaction 3). If present, the density of CH radicals should peak at a time delay governed by the ratio of the rate constants for the formation and loss processes. We looked for CH radicals over a range of time delays and over a range of atomic nitrogen concentrations by exciting the R1(1) line of the (1, 0) band of the $B^2\Sigma^- \leftarrow X^2\Pi_{1/2}$ transition at 363.080 nm and observing fluorescence around 404 nm via the (1, 1) band of the $B^2\Sigma^- \rightarrow X^2\Pi_{1/2}$ transition. Nevertheless, no fluorescence signal was ever seen at and around this wavelength, indicating that $C(^1D)$ formation is negligible under our experimental conditions.

Model cross-checks. The typical elemental abundance ratio (C/O) used by many authors is less than one so that a large amount of atomic oxygen is still available for the chemistry once CO has been formed. Depletion of oxygen compared to typical atomic abundances used has been proposed by Jenkins (2) based on the observation of atomic lines towards hundreds of lines of sight with different densities. Whittet (3) studied the budget of O-bearing species as a function of cloud density. In Fig. 3 of his article, he represented the fraction of the cosmic oxygen abundance that was observed in refractory grain cores, in the gas-phase (mainly in the form of CO), and in the ices. If one removes all these components, a large fraction of the oxygen is in an unidentified form that does not seem to participate in the chemistry. Hincelin et al. (4) used this hypothesis to explain the low O_2 gas-phase abundance in dense clouds. Considering the uncertainty on the oxygen elemental abundance to be used in dense clouds, two different values have been used for oxygen, leading to C/O elemental ratios of 0.7 and 1.2. All the model runs that we performed showed that the use of a low C/O elemental abundance ratio led to lower N_2 abundances, as explained by the influence of the O + CN reaction in the main article.

Other parameters, such as the choice of the initial conditions (initial species abundances), can be important for the model results. In our typical model, we start with all the species in atomic form, except for H_2, because we assume that dense clouds form from diffuse media where the elements are mostly in the atomic form. Nevertheless, molecules such as CO, OH, and CH are observed in diffuse clouds with abundances around 10^{-6} for CO and 10^{-8} ($/n_H$) for OH and CH (5, 6). The inclusion of these molecules in our models as initial conditions at their diffuse cloud abundances does not change the results for dense clouds.

The cosmic-ray ionization rate is another parameter that might change the model results. We tested its importance by running the model with two extreme values of the cosmic-ray ionization rate ζ: 10^{-18} and 10^{-16} s^{-1}. The predicted abundances of the major N-bearing species as a function of time computed with these values are shown in Fig. S3, for dense cloud conditions and depleted oxygen (C/O = 1.2). The age for which the model agrees with N_2H^+ observations in TMC-1 (CP) is clearly very dependent on this parameter. For a larger ζ than typically used (10^{-17} s^{-1}), the agreement between observations and models is obtained sooner (3–5 $\times 10^4$ yr) and the predicted abundance of N_2 at that time is smaller. A smaller cosmic-ray ionization rate produces an agreement at later times (8–10 $\times 10^5$ yr) and again the predicted abundance of gas-phase N_2 is smaller than for our typical model results.

We show in Fig. S1*B* the gas-phase abundances of CN and NO ($/n_H$) predicted by our model (c) for the two C/O elemental ratios. The CN abundance observed in TMC-1 (CP) is reasonably reproduced by our models, at the times defined by the N_2H^+

observations, considering the observed values of 6×10^{-8} ($/n_H$) of Ohishi (7) and Crutcher et al. (8), although a much smaller CN abundance of about 10^{-9} ($/n_H$) has been observed by Pratap et al. (9). The NO abundance observed in the same cloud by Gerin et al. (10) of 2.7×10^{-8} ($/n_H$) is also in agreement with our models.

The results of the prestellar core model (B68) using the C/O elemental ratio of 1.2 are shown in Fig. 5 and those for the C/O ratio of 0.7 are presented in Fig. S2, both for a time of 5×10^6 yr. This time was selected to reproduce the observed abundance of N_2H^+ in B68 (12). At early times, the model produces too much N_2H^+ whereas at later times, it produces too little of it. This time is very different from the one determined by Maret et al. (12) of 2×10^5 yr, but in their model all of the carbon was initially present as CO and the remaining oxygen was in the form of water ice; therefore,their timescale cannot be compared directly with ours. A few 10^6 yr for the "chemical" age of a prestellar core is in agreement with the conclusion of Pagani et al. (13) using deuterated species. In the case of prestellar cores, the choice of initial conditions can be debated since the material probably spent some time at intermediate densities during which some species are created. We tested this hypothesis by using the composition for a dense cloud computed by our model as the initial conditions for the prestellar core. We also ran simulations with half of the carbon already present as CO, keeping the rest in the atomic form. For these models, the results were similar to those shown in Fig. 5 and Fig. S2; however, the timescale to reach the observed N_2H^+ abundance was simply shifted towards smaller times. The main conclusion of this paper, that the use of up-to-date gas-phase chemistry decreases the fraction of nitrogen converted into N_2 at reasonable ages for both dense clouds and pre-stellar cores, appears to hold even for a wide range of initial model parameters.

1. Sato K, Ishida N, Kurakata T, Iwasaki A, Tsunashima S (1998) Reactions of C(^{1}D) with H_2, HD and D_2: Kinetic isotope effect and the CD/CH branching ratio. *Chem Phys* 237:195–204.
2. Jenkins EB (2009) A unified representation of gas-phase element depletions in the interstellar medium.*Astrophys J* 700:1299–1348.
3. Whittet DCB (2010) Oxygen depletion in the interstellar medium: Implications for grain models and the distribution of elemental oxygen. *Astrophys J* 710:1009–1016.
4. Hincelin U, et al. (2011) Oxygen depletion in dense molecular clouds: A clue to low O_2 abundance? *Astron Astrophys* 530:A61.
5. Lucas R, Liszt HS (2000) Comparative chemistry of diffuse clouds. I. C_2H and C_3H_2. *Astron Astrophys* 358:1069–1076.
6. Liszt HS, Lucas R (2002) Comparative chemistry of diffuse clouds. IV: CH. *Astron Astrophys* 391:693–704.
7. Ohishi M, Irvine WM, Kaifu N (1992) Molecular abundance variations among and within cold, dark molecular clouds in *IAU Symposium 150, Astrochemistry of Cosmic Phenomena*, ed Singh PD (Kluwer, Dordrecht), pp. 171–177.
8. Crutcher RM, Churchwell E, Ziurys LM (1984) CN in dark interstellar clouds. *Astrophys J* 283:668–674.
9. Pratap P, et al. (1997) A study of the physics and chemistry of TMC-1. *Astrophys J* 486:862–885.
10. Gerin M, VialaY, Casoli F (1994) The abundance of nitric oxide in TMC 1. *Astron Astrophys* 268:212–214.
11. Wakelam V, et al. (2012) A KInetic Database for Astrochemistry (KIDA). *Astrophys J Suppl Ser* 199:21.
12. Maret S, Bergin EA, Lada CJ (2006) A low fraction of nitrogen in molecular form in a dark cloud. *Nature* 442:425–427.
13. Pagani L, Roueff E, Lesaffre P (2011) Ortho-H_2 and the age of interstellar dark clouds. *Astrophys J Lett* 739:L35.
14. Womack M, Ziurys LM, Wyckoff S (1992) Estimates of N2 abundances in dense molecular clouds. *Astrophys J* 393:188–192.

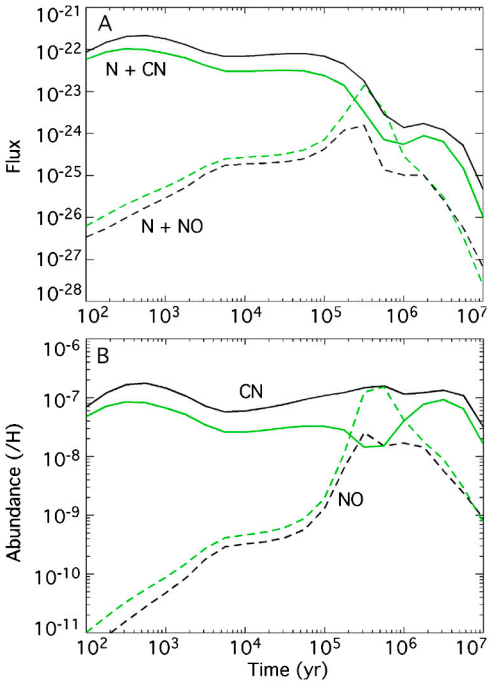

Fig. S1. Dense cloud model results for CN and NO molecules as a function of time. (*A*) Fluxes (the product of the rate constants and the densities of the two reactants) for the reactions N + NO and N + CN for dense cloud conditions using model (c) and for the elemental abundance ratios C/O of 1.2 (black lines) and 0.7 (green lines). (*B*) Gas-phase abundances of CN and NO ($/n_H$) with the same models as (*A*).

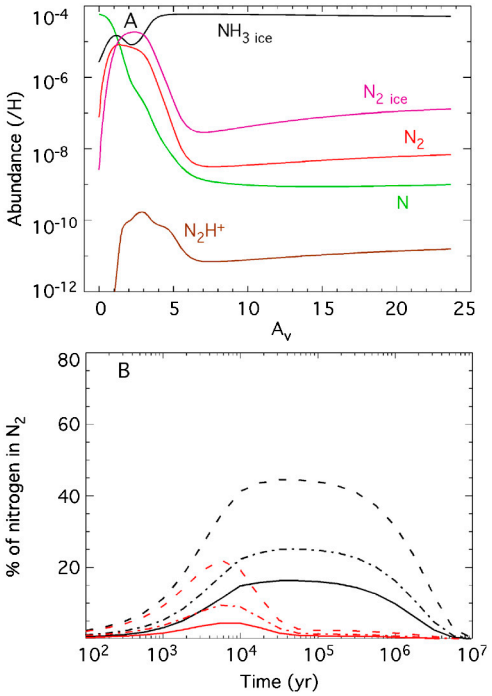

Fig. S2. Model results for the prestellar core B68 using a C/O elemental ratio of 0.7. (*A*) Gas phase abundances of N, N_2, N_2H^+, and ice abundances of N_2 and NH_3 ($/n_H$) as a function of visual extinction for model (c) at an age of 5×10^6 yr. (*B*) Percentage of elemental nitrogen in the form of N_2 (in the gas-phase and on interstellar ices) as a function of time. Red lines indicate gas-phase N_2 and black lines indicate total (gas + ice) N_2 with three different networks: dashed lines, model (a) OSU database; dashed-dotted lines, model (b) KIDA values (11); solid lines, model (c) KIDA with updates for reactions 1, 2, and 4.

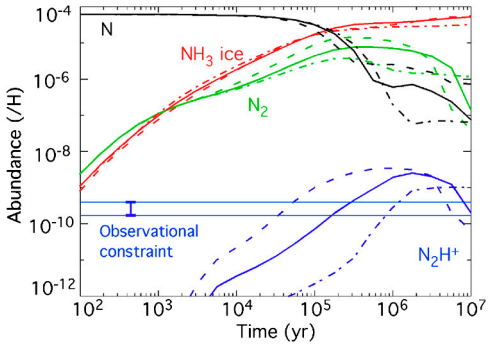

Fig. S3. Effect of the cosmic ray ionization rate on the fractional abundances of gas-phase N, N_2 and N_2H^+ and NH_3 ice ($/n_H$). Dense cloud physical conditions are used (total density $= 2 \times 10^4$ cm^{-3}) with different cosmic ray ionization rates: 10^{-18} s^{-1} (dashed-dotted lines), 10^{-17} s^{-1} (solid lines), and 10^{-16} s^{-1} (dashed lines). Horizontal blue lines represent the observational constraints on N_2H^+ from TMC-1 (CP) (9, 14).

Table S1. Measured rate constants, k_4, for the $N(^4S^0) + CN(^2\Sigma^+)$ reaction

T/K	$[N]/10^{14}$ cm^{-3}	Flow density/10^{16} cm^{-3}	N †	$k_4/10^{-11}$ cm^3 s^{-1}	$k'_4/k'_1 \equiv k_4/k_1$
56 ± 1	0.1 – 1.4 *	23.1 ± 0.1	66	4.9 ± 1.0	1.10 ± 0.04 ‡
87 ± 1	0.3 – 2.2	12.5 ± 0.1	54	4.8 ± 0.7	1.01 ± 0.03
152 ± 4	0.3 – 3.3	10.0 ± 0.1	67	6.9 ± 1.0	1.54 ± 0.03
169 ± 1	0.1 – 1.9	9.3 ± 0.2	84	6.9 ± 1.1	1.58 ± 0.04
296	0.4 – 2.8	16.0	58	9.0 ± 2.9	2.12 ± 0.06

*Range of nitrogen atom concentrations estimated from k'_1/k_1.

†Number of individual measurements.

‡The statistical uncertainties for the ratios k_1/k_4 at the level of one standard deviation from the mean, based on the number of measurements given in Table 1, were used to calculate the uncertainties on individual k_4 values. These statistical uncertainties were combined with the statistical uncertainties derived from measurements of k_1 by Daranlot et al. (1). Finally, a systematic uncertainty of 10% was added to this combined uncertainty to reach the error estimates for individual values of k_4.

1 Daranlot J, et al. (2011) Revealing atom-radical reactivity at low temperature through the N + OH reaction. *Science* 334:1538–1541.

Table S2. Initial model elemental abundances

Element	Abundance *	Element	Abundance
He	0.09	N	6.2×10^{-5}
C	1.7×10^{-4}	O	$(1.4, 2.4) \times 10^{-4}$
S	8×10^{-8}	Si	8×10^{-9}
Fe	3×10^{-9}	Na	2×10^{-9}
Mg	7×10^{-9}	Cl	1×10^{-9}
P	2×10^{-10}		

*Fractional abundances relative to elemental hydrogen.